Proc. of the 6th Intl. Symposium on Reliability Engineering and Risk Management (6ISRERM)
31 May – 1 June 2018, Singapore
Editor(s) Xudong Qian, Sze Dai Pang, Ghim Ping Raymond Ong, Kok-Kwang Phoon

ENERGY-BASED ANALYSIS OF MECHANISMS OF EARTHQUAKE-INDUCED LANDSLIDE

Gang Fan[1]; Li-Min Zhang[2]; Jian-Jing Zhang[3]; Fang Ouyang[4]

[1]*College of Water Resource and Hydropower, Sichuan University, Chengdu, P. R. China.*
E-mail: fangang@scu.edu.cn.
[2]*Department of Civil and Environmental Engineering, The Hong Kong University of Science and Technology, Hong Kong, P. R. China.*
E-mail: cezhangl@ust.hk.
[3]*Department of Geotechnical Engineering, Southwest Jiaotong University; Chengdu, Sichuan, P. R. China.*
E-mail: jianzhang1102@home.swjtu.edu.cn.
[4]*Department of Geotechnical Engineering, Southwest Jiaotong University; Chengdu, Sichuan, P. R. China.*
E-mail:ouyangfang26@126.com.

Based on the Hilbert-Huang Transform (HHT) and its marginal spectrum, an energy-based method for analyzing the dynamics of earthquake-induced landslides is proposed and a case study is presented in this study. The research results show that the seismic energy in the sliding mass is larger than that in the sliding bed when subjected to seismic excitations, causing different dynamic responses between the sliding mass and the sliding bed, which may be the most essential reason for the dynamic failure in the weak zone. The seismic energy moves from the high frequency components towards the low frequency components when the seismic waves propagate through the weak zone, causing nonuniform seismic energy distribution in the frequency domain. Shear failure develops first at the crest and the toe of the sliding mass due to the resonance effect, meanwhile, the seismic energy carried in the frequency components of 3-5 Hz, which is close to the natural frequency of the slope, is significantly dissipated in the initiation and failure processes of the landslide. With the development of dynamic failure, the peak energy transmission ratios of the weak zone decrease gradually. The study in this paper offers an energy-based interpretation for the initiation and failure mechanism of earthquake-induced landslides with the shattering-sliding failure type.

Keywords: Landslide, Seismic energy, Failure mechanism, Marginal spectrum

1 *Introduction*

Earthquake-induced landslides are one of the most destructive natural hazards and lead to enormous loss of property and lives around the world. The 12 May 2008 Wenchuan earthquake (Richter Scale M_L is 7.9) in western China triggered more than 56,000 landslides in steep mountainous terrains covering an area of about 41,750 km^2 (Dai et al. 2011). These landslides directly caused more than 20,000 fatalities (Yin et al. 2009). In recent years, many researchers paid their attention to landslide susceptibility (Ding and Hu 2014; Kayastha et al. 2012; Yishimatsu and Abe 2006; Chang et al. 2005), dynamic failure mechanisms (Guo and Hamada 2013; Huang et al. 2012; Li et al. 2012; Revellino et al. 2008; Zhou et al. 2013), etc. Many techniques have been utilized to analyze the dynamic stability and failure mechanisms of slopes. In fact, seismic energy is the fundamental trigger of landslide initiation and dynamic failure; therefore, it is extremely important to reveal the initiation and dynamic mechanisms of landslides from the viewpoint of seismic energy. In recent decades, some researchers have done some studies on the energy-based method in geotechnical engineering, including rock burst intensity classification (Chen et al. 2015), rock brittleness index and quantification (Munoz et al. 2016), energy dissipation and release during rock failure (Meng et al. 2016; Peng et al. 2015; Tang and Kaiser 1998; Zhang et al. 2000). However, the existing researches mainly focused on the static energy in the rock mass, very few studies are available on the seismic energy and energy-based method for initiation and failure mechanisms analysis of earthquake-induced landslides.

Since it was put forward by Huang et al. (1998), the Hilbert-Huang Transform (HHT) and its marginal spectrum have been widely adopted in many areas of geophysics. However, the HHT has not been fully utilized in geotechnical engineering. The existing studies indicate that this new decomposition technique is adaptive and highly efficient, and most importantly the HHT is very suitable for processing non-stationary and non-linear signals, e.g. earthquake waves. Based on the HHT, the marginal spectrum of the original signal can be obtained, which denotes the signal energy distribution in the frequency domains.

In the present study, based on the HHT signal processing technique and its marginal spectrum, large-scale shaking table tests and numerical simulations, an attempt is made to demonstrate the energy-based method in interpreting the dynamic mechanisms of earthquake-induced landslides with the shattering-sliding failure type.

2 *Energy-based analysis method*

The seismic energy, which can be quantitatively presented by the marginal spectra, is a trigger of the earthquake-induced landslides. Since a slope is characterized with dynamic features, the distribution of seismic energy in the frequency domain is significant for revealing the dynamic mechanisms of earthquake-induced landslides. Based on the concepts of the HHT and its marginal spectrum, the seismic energy distribution in the frequency domain can be identified.

When the seismic wave propagates through the slope with a weak zone, the seismic wave amplitude and the seismic energy distribution in the frequency domain will change significantly. On the one hand, the seismic energy amplitude at different parts of the slope will be different due to the complex reflection on the slope surface and refraction in the weak zone. On the other hand, the seismic energy distribution in the frequency domain will be influenced observably by the weak zone. Since the slope mass itself is characterized with dynamic features in the frequency domain, changes in the distribution of seismic energy in the frequency domain will affect the dynamic response of the slope undoubtedly, which will trigger the failure of the slope. By analyzing the change of seismic energy amplitude and seismic energy distribution in the frequency domain, combining with the observed phenomena in the initiation and failure processes of the earthquake-induced landslide, the initiation and failure mechanism can be revealed and interpreted from the viewpoint of seismic energy. For this reason, the proposed analysis method in this study can be defined as an energy-based method.

3 *Application of energy-based method to an earthquake-induced landslide*

3.1 *Geological conditions of the landslide*

The study landslide is located in the mountainous area in Guangyuan City, Sichuan Province, China. It was formed due to excavation and earthquake events. In the rainy seasons after the 12 May 2008 Wenchuan earthquake, the excavated slope started to slide at a rate of 1-2mm/d, and some tensile cracks were observed on the trailing edge of the landslide. The height of the landslide is 135m with an approximate topographical angle of 38°, the volume of the landslide is about 478,000m^3. The sliding bed is mainly formed with intact shale. The sliding mass consists of weathered shale and alluvial deposit, among which the alluvial deposit was excavated, hence the sliding mass only consists of weathered shale. The weak zone consists of silty clay.

In the past decade, two strong earthquakes struck this area, including 12 May 2008 Wenchuan earthquake and 20 April 2013 Lushan earthquake, both of which were induced by the Longmenshan fault zone in western China. The distance between the landslide and the Longmenshan fault zone is approximately 260km. Considering the importance of the site and constructions near the landslide, it is essential to reveal the dynamic mechanism of this landslide for hazard mitigation.

3.2 *Shaking table test*

The materials in the test model were mainly formed of sand, clay, plaster, water and barite at ratios of 1:0.6:0.5:0.28:0.8 for the sliding bed and 1:0.4:0.1:0.3:0.2 for the sliding mass. The materials in the test model were mixed according to the mix proportion obtained in previous laboratory experiments. The materials in the sliding zone were obtained from the prototype landslide and remodelled for the test model. The bottom surface size of the test model is 325 × 150cm and the height of the test model is 165cm. The length of the model slope is 325cm, which, according to existing studies (Liu et al. 2013, 2014), is an acceptable value for physical model test using a shaking table. In the test, a 5cm thick absorber made of foam materials was placed on the four sides of the rigid test box to minimize the influence of the container boundaries on the input seismic waves. Although the absorber may be considered to influence the displacements of the test model, Withman and Lambe (1986) and Liu et al. (2013, 2014) indicated that this approach allows for a “reasonably correct” boundary. The sizes and the layout of the acceleration monitoring points for the shaking table test are shown in Figure 1.

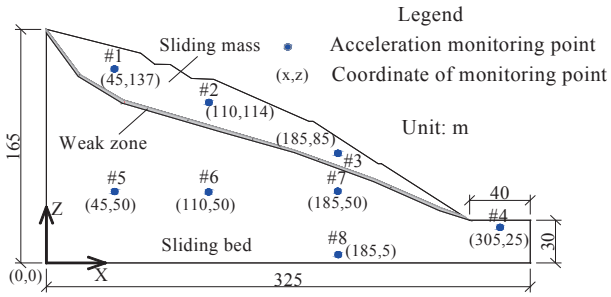

Figure 1 Full dimensions of the model slope and layout of the acceleration monitoring points

In reference to Buckingham's π theorem of similarity, the dimension L, mass density ρ, and acceleration a were chosen as the fundamental parameters with scaling factors of C_L=100, C_ρ=1 and C_a=1, respectively. After the test model was completed, samples were collected from the test model to obtain physical parameters in the laboratory. Uniaxial compression tests were performed to gain the elasticity modulus (E) and Poisson ratio (μ). Direct shear tests were performed to obtain the cohesive force (c) and internal friction angle (φ). The physical parameters of the test model are shown in Table 1.

Table 1 Material parameters

Material	Bulk modulus E (GPa)	Shear modulus G (MPa)	Density (g/cm^3)	Poisson's ratio	Cohesion (kPa)	Internal friction angle (°)
Sliding mass	1.67	0.77	2.1	0.3	8	60
Weak zone	0.0256	0.0073	1.95	0.37	15	22
Sliding bed	6.67	4	2.4	0.25	20	80

The loading waveform used in this shaking table test was an El Centro earthquake record, selected because it has been widely used in earthquake engineering around the world. According to the similarity criteria, the input earthquake records are compressed in the time axis at a compression ratio of 10 (the time similarity ratio).

Two simultaneous loading directions of experimental earthquake excitation were applied, namely the horizontal or X direction, and the vertical or Z direction. In this shaking table test, the horizontal peak accelerations of loading waveforms were scaled to 0.1g, 0.3g, 0.5g, 0.7g, and 0.9g. The model was subject to 0.1 g white noise scanning before the excitation of each input earthquake record. The natural frequency of the test model for X direction excitation is 3.55Hz.

3.3 *Analysis of seismic energy distribution*

The Hilbert spectra of all acceleration monitoring points, i.e. #1-#8, under the 0.3g El Centro earthquake wave show that the seismic energy distributes dispersedly in the time axis, but mainly in the range of 0-30s. #1, #2 and #3 acceleration monitoring points are all located in the sliding mass, the seismic energy distributes mainly in the frequency range of 0-5Hz, while the seismic energy of #4-#8 acceleration monitoring points, both of which are located in the sliding bed, distributes mainly in the frequency range of 0-10Hz. It also can be seen that the peak seismic energy amplitudes of #1, #2 and #3 acceleration monitoring points are larger than those of #4-#8.

According to the definition of marginal spectrum, the marginal spectrum of each acceleration monitoring point can be obtained. Taking the acceleration monitoring points in the sliding mass as examples, i.e. #1, #2 and #3, the marginal spectra of which under the excitations with 0.1g and 0.3g are calculated and shown in Figure 2, which shows that the marginal spectra curves of #1 and #3 are similar and different with the curves of #2. More specifically, the marginal spectrum curves of #1 and #3 have two peaks, the first of which appears in the frequency range of 1-2Hz, the second one appears in the frequency range of 3-5Hz. While the marginal spectrum curve of #2 has only one peak appearing in the frequency range of 1-2Hz, which coincides with the appearing frequency range of first peaks of #1 and #3. The peaks of #1, #2, and #3 in the frequency range of 1-2Hz are close and increase gradually with increasing input amplitude. In the frequency range of 3-5Hz, when the input amplitude reaches 0.3g, the peaks of marginal spectrum of #3 start to decrease, and suffer a drastic decrease when the input amplitude reaches 0.9g. Before the input amplitude reaches 0.7g, the peak of marginal spectrum of #1 increases gradually with increasing input amplitude, but the increasing ratio becomes smaller and smaller, finally suffers a drastic decrease when the input amplitude reaches 0.9g as well. The

peaks of marginal spectrum of #3 are larger than those of #1 in the frequency range of 3-5Hz, especially when subjected to 0.3g, 0.5g and 0.7g seismic excitations, as shown in Figure 3.

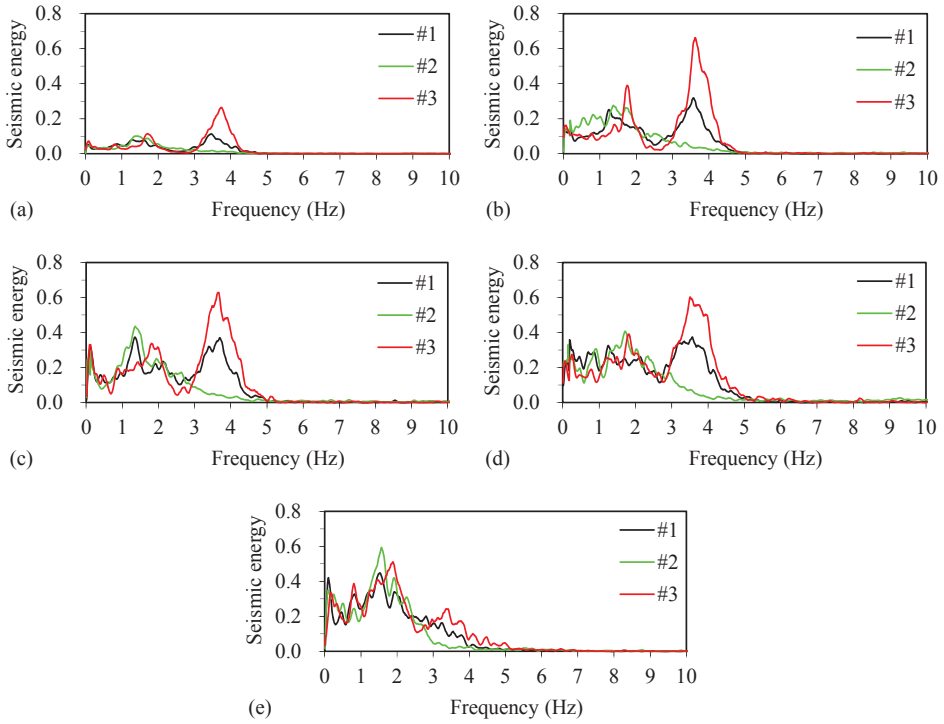

Figure 2 Marginal spectra of acceleration monitoring points in the sliding mass (#1, #2 and #3) under the El Centro earthquake waves with different amplitudes: (a) 0.1g; (b) 0.3g; (c) 0.5g; (d) 0.7g and (e) 0.9g

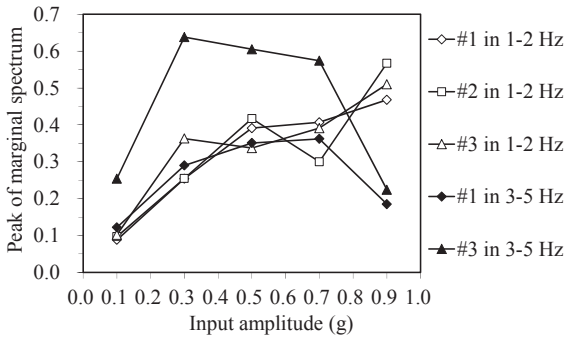

Figure 3 Variation of peaks of marginal spectra with the input amplitude in the frequency ranges of 1-2Hz and 3-5Hz

As the marginal spectrum offers a measure of total energy contribution from each frequency value, the area below the marginal spectrum curves in Figure 2 represents the total seismic energy over the entire frequency span. The total seismic energy of the monitoring points in the sliding mass, i.e. #1, #2 and #3, are calculated and shown in Figure 4. The total seismic energy of #5, #6 and #7 acceleration monitoring points, which are located in the sliding bed, are also calculated and shown in Figure 4 simultaneously for comparison. In the sliding mass, the total seismic energy of #3 is the largest and followed by #1, the total seismic energy of #2 is the smallest, which can be explained by that the seismic wave at #2 acceleration monitoring point does not carry much seismic energy in the frequency range of 3-5Hz, as shown in Figure 2. At the same time as it can be seen that the total seismic energy of the sliding mass is larger than that of the sliding bed. With the continuous excitation, the incident wave and the reflected wave would be superimposed when the incident wave reach the slope surface, causing the seismic energy stored in the sliding mass to be larger than that in the sliding bed.

The seismic energy in the sliding mass comes from the energy transmission of the weak zone; therefore, the study on the energy transmission ratio of the weak zone is essential for revealing and interpreting the dynamic

mechanism of the earthquake-induced landslides. In this study, energy transmission ratio is defined as the ratio of the marginal spectra in the sliding mass, i.e. #1, #2 and #3 acceleration monitoring points, to the marginal spectra in the sliding bed, i.e. #5, #6 and #7 acceleration monitoring points correspondingly. If the energy transmission ratio is larger than 1, it denotes an amplification effect, otherwise, it denotes an attenuation effect. The energy transmission ratios of the weak zone under different seismic wave excitations are calculated and shown in Fig. 5. To certify the influence of the weak zone on the seismic energy distribution in the frequency domain, the energy transmission ratios between #7 and #8 acceleration monitoring points, both of which are located in the sliding bed, are also calculated and shown in Figure 5.

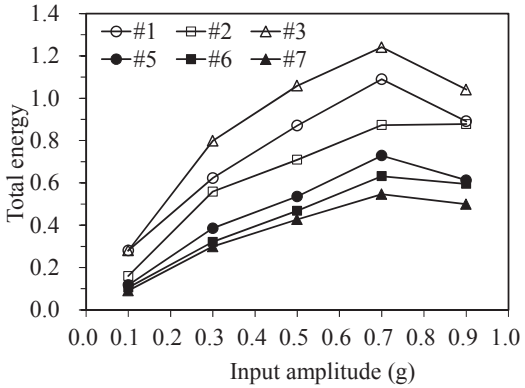

Figure 4 Total seismic energy of the acceleration monitoring points in the sliding mass (#1, #2 and #3) and the monitoring points in the sliding bed (#5, #6 and #7)

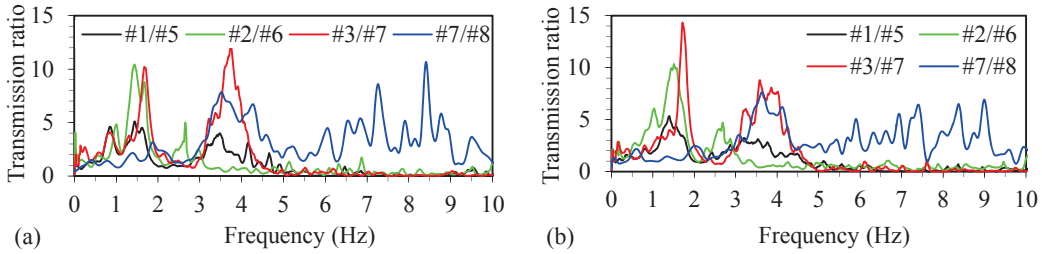

Figure 5 Transmission ratios of the marginal spectra under the El Centro seismic wave with different amplitudes: (a) 0.1 g; (b) 0.3 g

The energy transmission ratio between #7 and #8 acceleration monitoring points implies that the seismic energy in the frequency range of 3-9Hz is amplified observably when the seismic wave propagates in the sliding bed, especially in the frequency range of 7-9Hz. In the crest and the toe of the sliding mass, the seismic energy in the frequency ranges of 1-2Hz and 3-5 Hz is amplified, while in the middle part of the sliding mass, only the seismic energy in the frequency range of 1-2Hz is amplified. The seismic energy in the frequency range of larger than 5Hz is attenuated by the weak zone significantly when the seismic wave propagates through the weak zone. That is to say when the seismic wave propagates through the weak zone, the seismic energy carried in the high frequency components are attenuated and the seismic energy carried in the low frequency components are amplified, namely the seismic energy moves from the high frequency components towards the low frequency components. Due to the aforementioned amplification and attenuation effects of the weak zone, the seismic energy at the crest and the toe of the sliding mass is mainly carried in the frequency components of 1-2Hz and 3-5Hz, and the seismic energy at the middle part of the sliding mass is mainly carried in the frequency components of 1-2Hz, as shown in Figure 2. The analysis of the peak energy transmission ratios shows that the peak energy transmission ratios decrease gradually with increasing input amplitude, both in the frequency ranges of 1-2Hz and 3-5Hz, as shown in Figure 6.

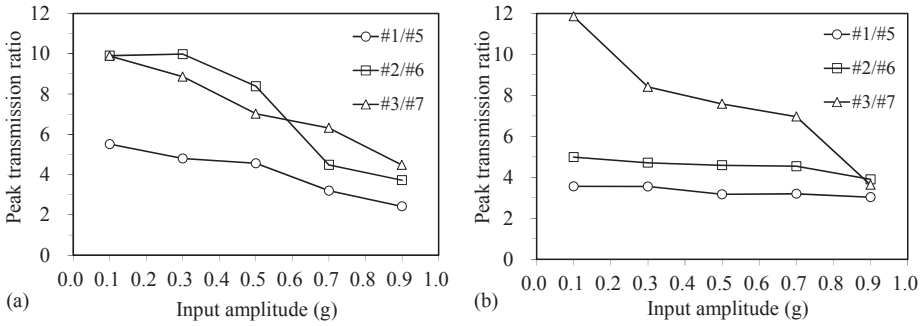

Figure 6 Peak energy transmission ratios along input seismic wave amplitude: (a) in the frequency range of 1-2Hz and (b) in the frequency range of 3-5Hz

4 *Conclusions*

Based on the research results in this study, several conclusions can be drawn:

(1) The seismic energy in the sliding mass is larger than that in the sliding bed due to the superposition of the incident wave and the reflected wave near the slope surface, leading to different dynamic responses between the sliding mass and the sliding bed.

(2) Because of the influence of the weak zone, the seismic energy moves from the high frequency components towards the low frequency components.

(3) In the slope crest and the slope toe, much seismic energy is carried in the frequency range of 3-5Hz, which is close to the natural frequency of the slope. The dynamic failure first develops at the slope crest and the slope toe due to the resonance response, and then extends towards the middle part of the weak zone. Finally a sliding surface forms and the slope slides.

(4) Since more and more seismic energy is dissipated in the weak zone during the forming of a slip zone, the peaks of the energy transmission ratios decrease gradually with increasing input amplitude.

References

Chang, K.J., Taboada, A., Lin, M.L., and Chen, R.F., Analysis of landsliding by earthquake shaking using a block-on-slope thermo-mechanical model: Example of Jiufengershan landslide, central Taiwan, *Eng. Geol*., 80, 151-163, 2005.

Chen, B.R., Feng, X.T., Li, Q.P., Luo, R.Z., and Li, S.J., Rock burst intensity classification based on the radiated energy with damage intensity at Jinping□hydropower station, China, *Rock Mech. Rock Eng.*, 48, 289-303, 2015.

Dai, F.C., Xu, C., Yao, X., Xu, L., Tu, X.B., and Gong, Q.M., Spatial distribution of landslides triggered by the 2008 Ms 8.0 Wenchuan earthquake, China, *J. Asian Earth Sci.*, 40,883-895, 2011.

Ding, M.T., and Hu, K.H., Susceptibility mapping of landslides in Beichuan County using cluster and MLC methods, *Nat. Hazards*, 70,755-766, 2014.

Guo, D., and Hamada, M., Qualitative and quantitative analysis on landslide influential factors during Wenchuan earthquake: A case study in Wenchuan County, *Eng. Geol.*, 152, 202-209, 2013.

Huang, N.E., Shen, Z., Long, S.R., Wu, M.C., Shih, H.H., Zheng, Q.A., Yen, N.C., Tung, C.C., and Liu, H.H., The empirical mode decomposition and Hilbert spectrum for nonlinear and non-stationary time series analysis, *Proceeding of the Royal Society* A 454, 903-995, 1998.

Huang, R.Q., Pei, X.J., Fan, X.M., Zhang, W.F., Li S.G., and Li, B.L., The characteristics and failure mechanism of the largest landslide triggered by the Wenchuan earthquake, May 12, 2008, China, *Landslides*, 9,131-142, 2012.

Kayastha, P., Dhital, M.R., and Smedt, F.D. Landslide susceptibility mapping using the weight of evidence method in the Tinau watershed, Nepal, *Nat. Hazards*, 63,479-498, 2012.

Li, X.P., He, S.M., Luo, Y., and Wu, Y., Simulation of the sliding process of Donghekou landslide triggered by the Wenchuan earthquake using a distinct element method, *Environ. Earth Sci.*, 65,1049-1054, 2012.

Liu, H.X.，Xu, Q., and Li, Y.R., Effect of Lithology and Structure on Seismic Response of Steep Slope in a Shaking Table Test, *J. Mt. Sci.*, 11(2), 371-383, 2014.

Liu, H.X., Xu, Q., Li, Y.R., and Fan, X.M., Response of High-Strength Rock Slope to Seismic Waves in a Shaking Table Test, *B. Seismol Soc. Am.*, 103, 3012-3025, 2013.

Meng, Q.B., Zhang, M.W., Han, L.J., Pu, H., and Nie, T.Y., Effects of acoustic emission and energy evolution of rock specimens under the uniaxial cyclic loading and unloading compression, *Rock Mech. Rock Eng.*, 49,3873-3886, 2016.

Munoz, H., Taheri, A., and Chanda, E.K., Fracture energy-based brittleness index development and brittleness quantification by pre-peak strength parameters in rock uniaxial compression, *Rock Mech. Rock Eng.*, 49, 4587-4606, 2016.

Peng, R.D., Ju, Y., Wang, J.G., Xie, H.P., Gao, F., and Mao, L.T., Energy dissipation and release during coal failure under conventional triaxial compression, *Rock Mech. Rock Eng.*, 48, 509-526, 2015.

Revellino, P., Guadagno, F.M., and Hungr, O., Morphological methods and dynamic modeling in landslide hazard

assessment of the Campania Apennine carbonate slope, *Landslides*, 5,59-70, 2008.

Tang C.A., and Kaiser, P.K., Numerical simulation of cumulative damage and seismic energy release during brittle rock failure - part I: fundamentals, *Int. J. Rock Mech. Min*., 35,113-121, 1998.

Whitman, R., and Lambe, P., Effect of boundary conditions upon centrifuge experiments using ground motion simulation, *Geotechl. Test J.*, 9, 61-71, 1986.

Yin, Y.P., Wang, F.W., and Sun, P., Landslide hazards triggered by the 2008 Wenchuan earthquake, Sichuan, China, *Landslides*, 6, 139-152, 2009.

Yoshimatsu, H., and Abe, S., A review of landslide hazards in Japan and assessment of their susceptibility using an analytical hierarchic process (AHP) method, *Landslides*, 3, 149-158, 2006.

Zhang, Z.X., Kou, S.Q., Jiang, L.G., and Lindqvist, P.A., Effects of loading rate on rock failure: failure characteristics and energy partitioning, *Int. J. Rock Mech. Min*. 37,745-762, 2000.

Zhou, J.W., Cui, P., and Fang, H., Dynamic process analysis for the formation of Yangjiagou landslide-dammed lake triggered by the Wenchuan earthquake, China, *Landslides*, 10, 331-342, 2013.